

## LIF measurements of scalar mixing in turbulent shear layers

By P. S. Karasso<sup>1</sup> AND M. G. Mungal<sup>1</sup>

### 1. Motivation and objectives

The structure of shear layer flows at high Reynolds numbers remains a very interesting problem. Straight mixing layers have been studied (Brown & Roshko, 1974, Dimotakis & Brown, 1976, Konrad, 1977, Mungal *et al.*, 1985) and yielded information on the probability density function (pdf) of a passive scalar across the layer. Konrad (1977) and Koochesfahani & Dimotakis (1986) measured the pdf of the mixture fraction for mixing layers of moderate Reynolds numbers, each about 25,000 ( $Re$  based on velocity difference and visual thickness). Their measurements showed a "non-marching" pdf (central hump which is invariant from edge to edge across the layer), a result which is linked to the visualizations of the spanwise Kelvin-Helmholtz (K-H) instability mode, which is the primary instability for plane shear layer flows. Similar measurements at higher Reynolds numbers remain an open question: a "marching" behavior of a passive scalar pdf at  $Re = 70,000$  by Batt (1977) suggests either resolution problems of the measurements or a change in the physical mechanisms of entrainment and mixing.

A secondary instability mode, the Taylor-Görtler (T-G) instability, which is associated with streamwise vortical structures, has also been observed in shear layers (Bernal & Roshko, 1986, Breidenthal, 1981, Konrad, 1977, Lasheras & Choi, 1988). Image reconstruction by Jimenez *et al.* (1985) and volume renderings by Karasso & Mungal (1990) at low  $Re$  numbers have demonstrated that the K-H and the T-G instability modes occur simultaneously in a non-mutually destructive way, evidence that supports the quasi two-dimensional aspect of these flows and the non-marching character of the pdf at low Reynolds numbers. At higher  $Re$  numbers though, the interaction of these two instability modes is still unclear and may affect the mixing process.

The shear layer is also known to be very sensitive to its initial conditions (Bradshaw, 1966, Browand & Latigo, 1979, Mungal *et al.*, 1985), which eventually determine the transition to turbulence. Furthermore, Huang & Ho (1990) found that the generation and transition to small-scale eddies occurs through vortex pairings. They showed that the transition to the fully developed regime is correlated with the number of large-scale structure pairings which depend on the operating conditions, namely the speed ratio, the first instability wavelength, and the downstream location. Their findings have great implications to the present study since it is the small scales that effect the passive scalar mixing process.

<sup>1</sup> Stanford University

In this study, we perform measurements of the concentration pdf of plane mixing layers for different operating conditions. At a speed ratio of  $r = U_1/U_2 = 4 : 1$ , we examine three Reynolds number cases:  $Re = 14,000$ ,  $Re = 31,000$ , and  $Re = 62,000$ . Some other  $Re$  number cases' results, not presented in detail, will be invoked to explain the behavior of the pdf of the concentration field. A case of  $r = 2.6 : 1$  at  $Re = 20,000$  is also considered. The planar laser-induced fluorescence technique is used to yield quantitative measurements. The different  $Re$  are obtained by changing the velocity magnitudes of the two streams. The question of resolution of these measurements will be addressed. In order to investigate the effects of the initial conditions on the development and the structure of the mixing layer, the boundary layer on the high-speed side of the splitter plate is tripped. The average concentration and the average mixed fluid concentration are also calculated to further understand the changes in the shear layer for the different cases examined.

## 2. Accomplishments

### 2.1. Experimental procedure

#### 2.1.1 Facility

The facility consists of a blow-down water tunnel, the schematic and details of which appear in Karasso & Mungal (1990). The overhead tank is partitioned so that one side can be uniformly seeded with fluorescent dye. The facility can be operated at various speed ratios.

#### 2.1.2 Experimental Technique

The planar laser-induced fluorescence (PLIF) technique (Kychakoff *et al.*, 1984, Pringsheim, 1949) is used to acquire quantitative images of the concentration field across the layer. PLIF is a powerful, non-invasive technique with good temporal and spatial resolution. The low-speed stream is seeded with a fluorescent dye, 5(6)-carboxy 2'7'-dichlorofluorescein. The choice of dye will be discussed shortly. A thin laser light sheet (about  $400 \mu\text{m}$ ) is generated from a 1.5 W Nd:Yag laser and is oriented in the streamwise direction. A 2-D CCD array is used to record the fluorescence signals. The camera collects the light at a right angle with respect to the plane of the laser sheet. Appropriate filters are placed in front of the camera lens (Nikon 50mm,  $f = 1.8$ ) to ensure that only fluorescence signals are recorded on the imaging array. The images are acquired (8 bits) and stored on a computer.

#### 2.1.3 Signal calibrations

The choice of a pulsed laser was made on the basis of improving the temporal resolution of the measurements. Each pulse of the present Nd:Yag laser (532 nm) has a duration of about 10 ns. The fluorescence lifetime is of the same order. The smallest time scale for mixing for all the experimental cases is on the order of microseconds. Our images can then be characterized by superior temporal resolution.

In the past, sodium fluorescein (in combination with CW lasers) was used as a fluorescent dye for quantitative measurements in similar experiments (Dahm, 1985, Koochesfahani *et al.*, 1986, Walker, 1987). The absorptivity of sodium fluorescein,

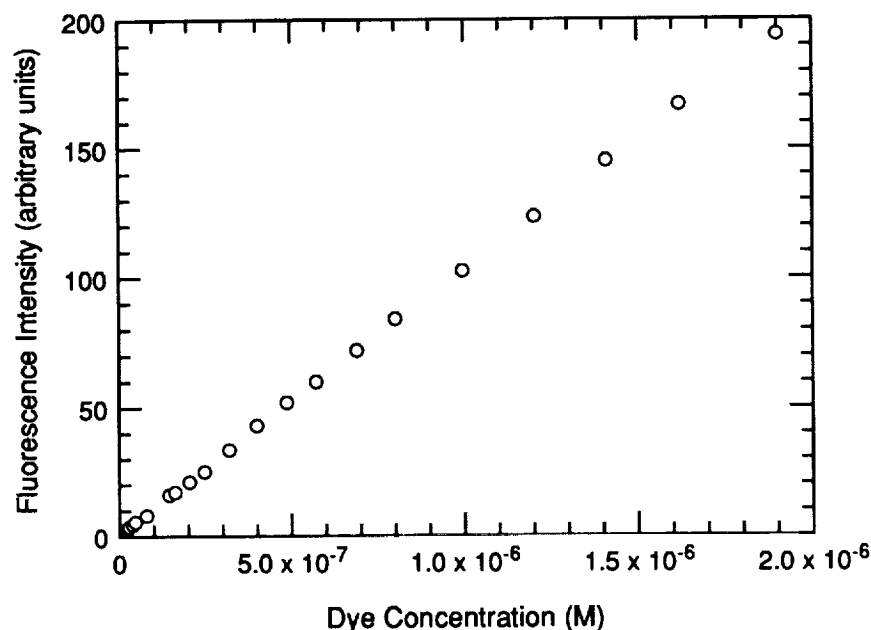


FIGURE 1. Fluorescence intensity vs. dye molar concentration.

though, at 532 nm (Nd:Yag) is significantly decreased (consult absorption spectrum, not shown here). This means that in order to produce, with the Nd:Yag laser, sufficient for imaging fluorescence signals, we would have to either increase the pumping power of the laser or increase the dye concentration. Both suggestions proved not well suited for quantitative imaging since they drove the fluorescence signal into the non-linear regime with dye concentration or with laser energy.

A different dye, 5( & 6)-carboxy2'7'-dichlorofluorescein, was then chosen. Considerations for choosing a dye include solubility in water and avoidance of optical trapping. A linearity check of the fluorescence signal intensity vs. dye concentration (the quantity that is ultimately measured) was performed. The result appears in Figure 1. The response is linear for the range of dye concentrations we used in this experiment. This test also implied that no measurable photobleaching would occur for a flowing system. Furthermore, we ensured that the response of the signal was linear with the laser energy used; although a higher (than that actually used) dye concentration would optimize the fluorescence signal for the input laser energy, a lower signal level was obtained (decreased dynamic range) in order to compensate for the high cost of the dye.

For all runs, a dye concentration of  $1.5 \times 10^{-6}$  M was implemented in seeding the low-speed side. An overall long focal length lens system was used to generate the laser sheet in order to minimize sheet-thickness variations across the imaged region. Also, the sheet was overexpanded in order to minimize the corrections needed to account for the spatial variation of the intensity of the laser light.

### 2.2. Experimental conditions

For all the acquired images, the actual size of the imaged region is about 7.0 x 5.2 cm. Hence the imaged area on each pixel of a digitized image is 137  $\mu\text{m}$  by 217  $\mu\text{m}$ . These numbers represent nominal values since the actual spatial resolution is determined by the "worst" dimension, which for this case is either the laser sheet thickness (about 400  $\mu\text{m}$ ) or the fact that a Nyquist sampling filter should be applied when digitization occurs, thus reducing the pixels' resolution by a factor of two. Additional factors that may limit the spatial resolution of the acquired images include focusing and camera alignment.

A first set of experiments at a speed ratio of  $r = 4 : 1$  were performed. Three different cases were examined, corresponding to a high-speed stream velocity magnitude  $U_1$  of 0.34 m/s, 0.90 m/s and 1.80 m/s. The estimated (using Thwaite's method) boundary layer momentum thicknesses  $\theta$  on the high-speed side at the splitter plate tip are 0.030 cm, 0.020 cm, and 0.015 cm, respectively. The center of each image is located at 25 cm downstream of the splitter plate (the visual thickness of the layer at this location has been used to assign a Reynolds number to each case). A second set of experiments was performed at the same speed ratio and the same three velocity magnitude values by placing a 1.5 mm diameter (trip) rod at the high-speed side of the splitter plate at a location of about 6 cm upstream of the tip. Finally, a case of a speed ratio of  $r = 2.6 : 1$  and  $U_1 = 0.67$  m/s and another one of  $r = 4 : 1$  and  $U_1 = 0.75$  m/s were also run.

### 2.3. Results

About 100 images represent the data used to extract results for the composition field for each case. By averaging all the images for each case, we obtain the visual thickness ( $\delta$ ) of the layer at 25 cm downstream of the splitter plate. Thus, for the untripped boundary layer cases of  $r = 4 : 1$  we find:

$$U_1 = 0.34\text{m/s} \quad : \quad \delta = 5.3\text{cm} \quad ; \quad Re \sim 14,000$$

$$U_1 = 0.90\text{m/s} \quad : \quad \delta = 4.7\text{cm} \quad ; \quad Re \sim 31,000$$

$$U_1 = 1.80\text{m/s} \quad : \quad \delta = 4.3\text{cm} \quad ; \quad Re \sim 62,000$$

These Reynolds numbers will be also used to label the tripped cases with similar velocity magnitudes (although the actual  $Re$  for the tripped cases is different since the size of the layer changes). When averaging the images for the tripped cases, the following visual thicknesses are obtained ( $r = 4 : 1$ ):

$$U_1 = 0.34\text{m/s} \quad : \quad \delta_{tr} = 5.4\text{cm}$$

$$U_1 = 0.90\text{m/s} \quad : \quad \delta_{tr} = 3.6\text{cm}$$

$$U_1 = 1.80\text{m/s} \quad : \quad \delta_{tr} = 3.6\text{cm}$$

It is seen that the layer shrinks on average by about 20% for the tripped cases for the higher  $Re$  (also see Browand & Latigo, 1979).

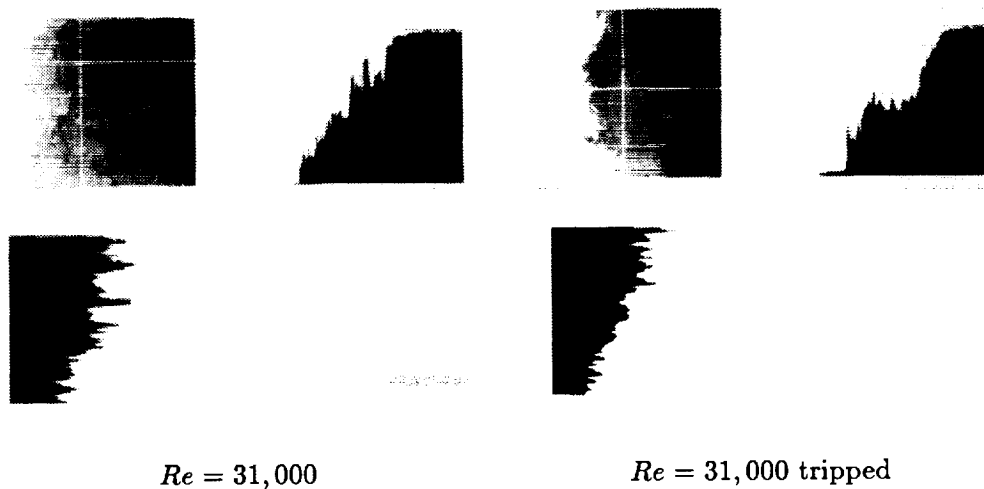


FIGURE 2. Images (7cm x 5 cm) of the mixing layer at speed a ratio of 4:1. Flow is from top to bottom. Streamwise and cross-stream cuts show concentration distributions.

Two examples of (corrected) images are shown in Figure 2. Perpendicular cuts in the streamwise and the cross-stream direction are shown on the right and bottom of each image and represent the distribution of the concentration field. The concentration field across the layer can be uniform or can have strong ramps. The pictures depict organized motion, but loss of organization was also observed, for all the cases. The structures tend to be more uniform in concentration at  $Re = 14,000$ . The concentration ramps were more frequently encountered at the two higher  $Re$  cases (for both tripped and untripped), even when the images displayed strongly organized motion dominated by a K-H roll. For structures of uniform concentration, there was also structure-to-structure variation. This suggests that there is some periodicity or non-uniformity in the amount of entrained fluid in the mixing layer, a result which is not surprising given the fluctuating nature of turbulent flows.

The pdf of the mixture fraction  $\xi$  at a given location  $y$  across the layer is defined as:

$$\text{Probability} = P(\xi \leq \xi(y) \leq \xi + \Delta\xi)$$

The pdf results for all cases of  $r = 4 : 1$  are shown in Figure 3. The calculated average concentration (mean) and average concentration of mixed fluid (mixed mean) are shown in Figure 4. In defining the mean mixed, concentration values to within 15% of the free streams' values were considered to be pure unmixed fluid. [Note: throughout this work,  $\xi = 1$  corresponds to the low-speed side fluid.]

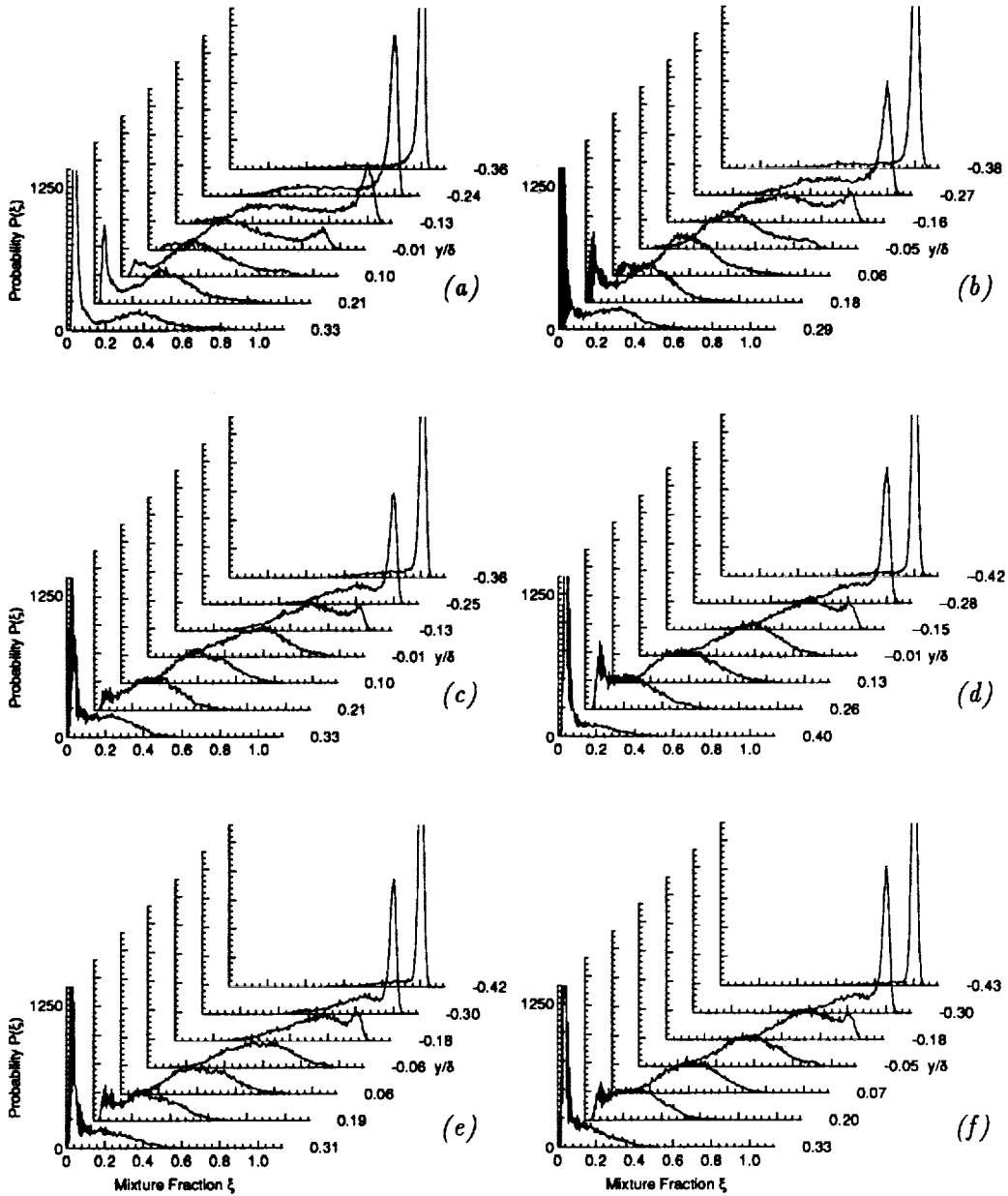


FIGURE 3. Probability distribution function of the mixture fraction  $\xi$  across the mixing layer. Speed ratio 4:1. (a)  $Re=14,000$ . (b)  $Re=14,000$  [tripped]. (c)  $Re=31,000$ . (d)  $Re=31,000$  [tripped]. (e)  $Re=62,000$ . (f)  $Re=62,000$  [tripped].

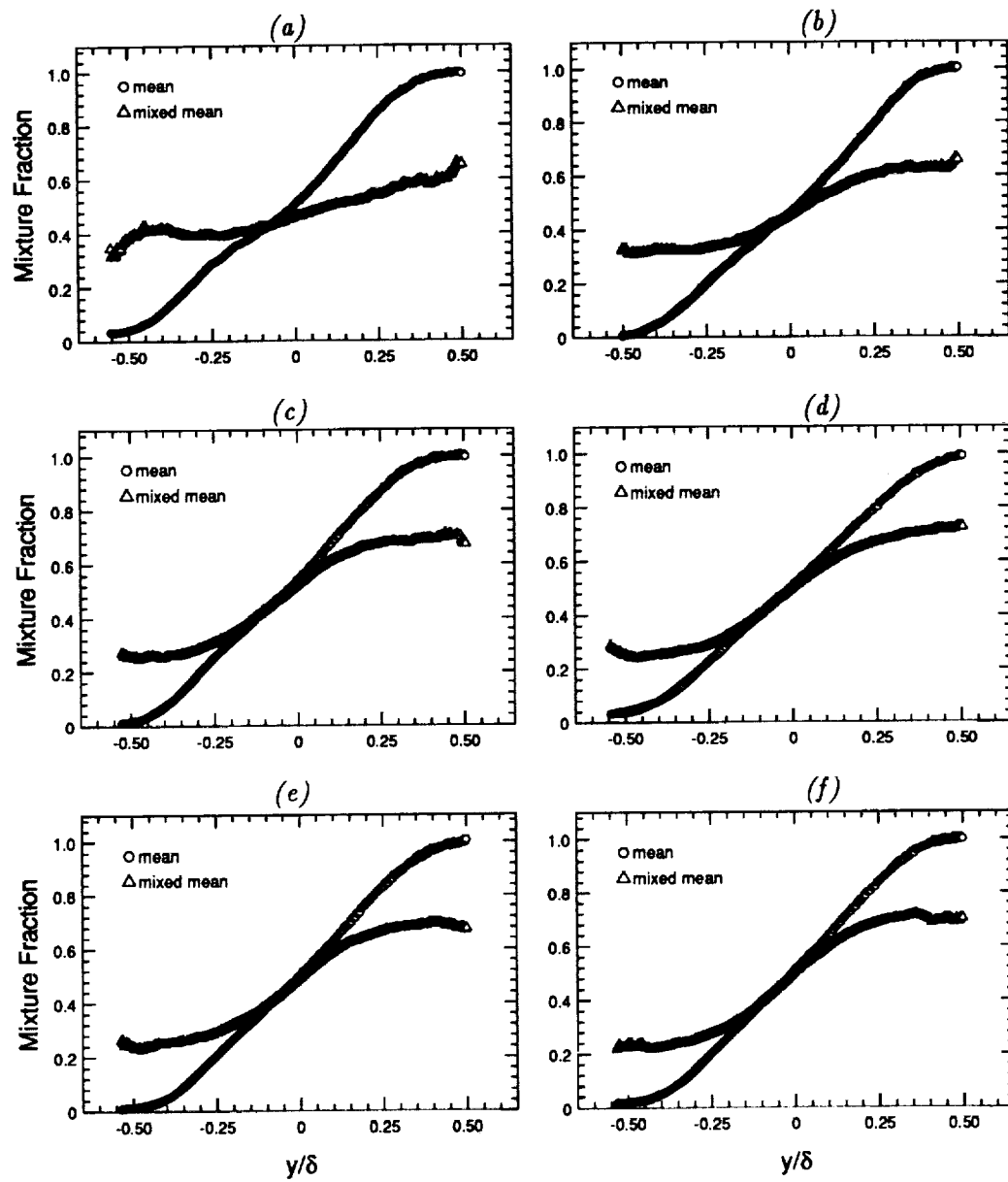


FIGURE 4. Mean and mixed mean fluid concentration across the layer. Speed ratio 4:1. (a) Re=14,000. (b) Re=14,000 [tripped]. (c) Re=31,000. (d) Re=31,000 [tripped]. (e) Re=62,000. (f) Re=62,000 [tripped].

For the  $Re = 14,000$  case, the pdf is non-marching (Fig. 3a). A broad range of concentration values is found at each location across the layer. We attribute this phenomenon to both streamwise concentration ramps and to the structure-to-structure variation. In the tripped  $Re = 14,000$  case (Fig. 3b), the non-marching feature is essentially preserved, although a small variation of the peak can be observed while moving across the layer. The mean and the mixed mean fluid concentrations are shown in Figure 4a. For the mean concentration, a triple inflection point is evident. This kind of behavior was also noticed by other investigators (Konrad, 1977, Koochesfahani & Dimotakis, 1986), suggesting that the large scale structures affect the way the mixing layer develops. For the mean mixed concentration curve, we notice a much smaller variation across the layer, a result of the fact that large-scale structures dominate the flow. For the tripped case (Fig. 4b), there is little evidence of a triple inflection point, suggesting a shift in the way the large-scale structures influence the growth of the layer.

For the  $Re = 31,000$  and the  $Re = 62,000$  cases, we notice a broad-marching type pdf of the mixture fraction (Fig. 3c, 3e). The two cases look very similar to each other but very different from the  $Re = 14,000$  case. The above is true for both the untripped and the tripped (Fig. 3d, 3f) boundary layer cases. The mean and the mixed mean concentrations (Fig. 4c, 4d, 4e, 4f) still have a much different slope, suggesting that large-scale structures still play an important role in the development of the shear layer. These structures, though, have streamwise concentration ramps which account for the broad-marching behavior of the pdf. It must be noted that K-H rolls were evidenced for all cases up to the highest  $Re$  number case examined.

A case of  $Re = 27,000$  at the same speed ratio ( $r = 4 : 1$ ) was examined and yielded a broad-marching type pdf similar to the marching type ones that were just presented. This result seems to be in contrast to that of Koochesfahani and Dimotakis if only the  $Re$  number is considered to characterize the flows. However, the difference in the speed ratio and hence the difference in the magnitudes of the velocities needed to produce the same  $Re$  account for different initial conditions and hence different layers; a more detailed explanation is given at a subsequent section. Furthermore, a case of  $r = 2.6 : 1$  at  $Re = 20,000$  yielded a non-marching type pdf.

Finally, as one moves to higher  $Re$ , the issue of relative resolution could dominate the outcome of the results; we hence address it in the following section.

#### *2.4 Issue of resolution*

The smallest spatial fluid mechanical scale characterizing the flow is the diffusive scale  $\lambda$  (Batchelor's scale), which is given by

$$\lambda/\delta = Sc^{-1/2} * Re^{-3/4}$$

For the cases of interest in this experiment, the following  $\lambda$ 's are estimated at the location of the measurements (using a constant of proportionality equal to one):

$$U_1 = 0.34\text{m/s} \quad ; \quad \lambda \sim 1.7\mu\text{m}$$

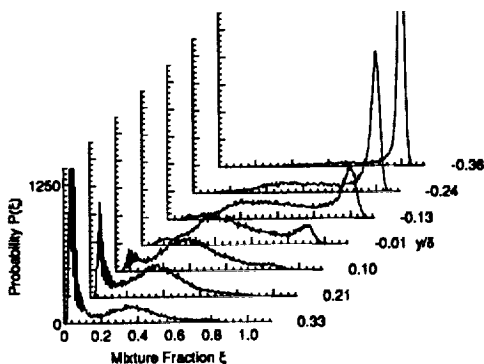


FIGURE 5. Probability distribution function of the  $Re = 14,000$  case with decreased spatial resolution.

$$U_1 = 0.90\text{m/s} \quad ; \quad \lambda \sim 0.8\mu\text{m}$$

$$U_1 = 1.80\text{m/s} \quad ; \quad \lambda \sim 0.4\mu\text{m}$$

We notice how these numbers are significantly smaller than the sampled area of our measurements ( $\Delta x = 137\mu\text{m}$ ,  $\Delta y = 237\mu\text{m}$ ). In order to address the possibility of resolution masking the real mixing field and biasing the pdf results, we artificially worsen the resolution of the untripped  $Re = 14,000$  case, via data sample binning, by a factor of two to make it similar to the  $Re = 31,000$  case. The result appears in Figure 5. The non-marching character is essentially unchanged (compare with Fig. 3c). We believe that the ramps that are observed at the higher  $Re$  number cases, in spite of the decreased resolution of the measurements, are a real phenomenon associated with the evolution of the flow, and that the pdf's reflect this behavior.

### 2.5. Discussion

According to Huang & Ho (1990), the production of small-scale eddies is associated with the interaction of the K-H with the T-G structures. The vortex pairings, which eventually lead to a transition to the fully developed regime, occur at a location which depends on the operating conditions. They used the non-dimensional parameter  $Rx/\lambda$  to show the evolution of the roll-off exponent of the velocity power spectra,  $n$ , to its asymptotic value, and to denote the location of the vortex merging [ $R = (1 - r)/(1 + r)$ ,  $x$  is the downstream from the splitter plate location and  $\lambda$  is the initial instability wavelength; [ $\lambda \sim 30\theta$ ]. Their plot is reproduced in Figure 6. We shall refer to  $Rx/30\theta$  as the "pairing parameter".

We then mark on this plot the present experiments as well as the one by Koochesfahani & Dimotakis according to their corresponding value of  $Rx/30\theta$ . We notice that all cases corresponding to a value of the pairing parameter of less than about 20 have a non-marching type pdf of the mixture fraction, whereas the ones above 20 have a marching type pdf. It is interesting to note that on this plot, experiments of similar  $Re$  numbers can differ in their  $Rx/30\theta$  value, thus yielding different types of pdf. The mixing transition (Breidenthal, 1981, Konrad, 1977, Koochesfahani

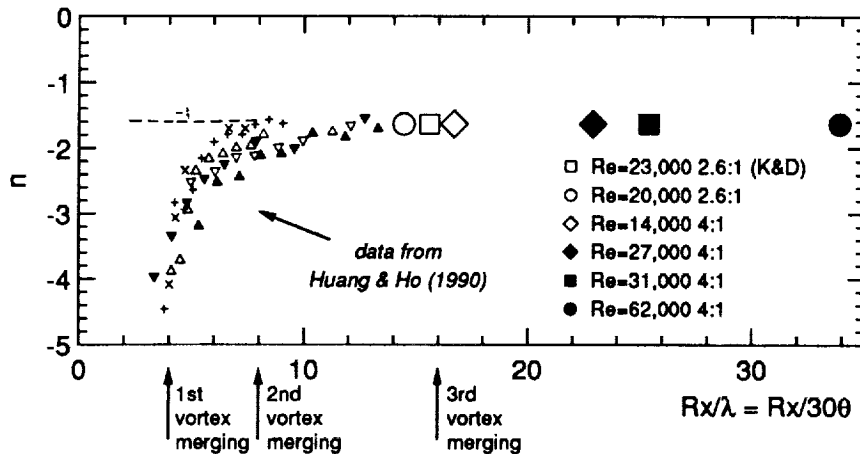


FIGURE 6. Roll-off exponent of velocity power spectra  $n$  vs. pairing parameter. (from Huang & Ho).

& Dimotakis, 1986), whereby the amount of molecular mixing is increased, is now logically associated with the second vortex merging. The transition to the fully developed regime is no longer a function of the  $Re$  number only, but of the non-dimensionalized distance  $Rx/30\theta$  at which sufficient action of vortex merging has led to the generation of small-scale eddies. In particular, our results combined with those of Huang & Ho suggest that the layer yields its asymptotic pdf at locations greater than three vortex mergings. Whereas boundary layer tripping has an effect on the development and growth of the mixing layer for all the cases examined and affects the pdf at a low value of the pairing parameter, it appears to have no effect on the shape of the pdf once the layer is fully developed. It is to be understood that parameters such as the free stream turbulence level or the aspect ratio of the test section, which differ for different facilities, may modify the above pairing parameter value of 20. The important point to be made, though, is that the  $Re$  number alone is not a sufficient parameter to characterize shear layers and that fully developed shear layers have, we believe, a broad-marching type pdf.

### 2.6. Conclusions

Experiments were performed to investigate the dependence of the structure of the shear layer on the operating conditions. We found that the concentration pdf shows a non-marching behavior at an initial stage but eventually develops to a broad-marching type pdf for fully developed layers. The  $Re$  number alone is not adequate to characterize whether or not the layer is fully developed: parameters such as the speed ratio and the initial boundary layer momentum thickness are equally important in determining the character of the passive scalar mixing field in shear layers. The value of the pairing parameter, which also correlates with the large-scale structure merging and the transition to small-scale eddies as found by Huang & Ho, seems to offer a criterion in determining the pdf behavior of plane

mixing layers. The second vortex merging appears to be associated with the mixing transition and a non-marching pdf. The third vortex merging defines the fully developed, broad-marching pdf. Well defined, organized large-scale structures were observed for all the cases (tripped and untripped boundary layers, all  $Re$  numbers). The structures developed concentration ramps as the layer evolved into the fully developed regime. The broad range of mixture fraction values that were found is associated with structure-to-structure variation. Finally, the mean and the mixed mean concentrations suggest that the large-scale structures affect the overall mixing process.

### 3. Future work

The interpretation of the structure of the mixing layer through the large-scale structures, and thus through the Kelvin-Helmholtz and the Taylor-Görtler instabilities, lead us to the question: can mixing enhancement be achieved by "adjusting" the strength of either the T-G or the K-H instability mode? To answer this, we intend to measure the pdf of the mixture fraction of longitudinally curved mixing layers. In a curved mixing layer, placing the high-speed stream on the inside of the bend (unstable) enhances the T-G instability mode, whereas placing it on the outside of the bend (stable) suppresses the T-G. Thus, our goal is to measure in detail the pdf of the mixture fraction for stable and unstable mixing layers, with differences in the pdf's reflecting differences in the mechanism of the mixing process as produced by the competition of the two instability modes.

The passive scalar technique has an additional inherent resolution problem in that it cannot distinguish mixed from unmixed (stirred) fluid within the sampling volume but will yield an average intensity (Breidenthal, 1981). A chemical reaction technique will be implemented in the future to address this issue and the changes that can result in the pdf.

### Acknowledgements

The authors wish to thank Dr. Jerry M. Seitzman for his help and discussions. Finally, the authors wish to thank Professor R. K. Hanson for the use of the Pixar Imaging System.

### REFERENCES

- BATT, R. G. 1977 Turbulent Mixing of Passive and Chemically Reacting Species in a Low-Speed Shear Layer. *J. Fluid Mech.* **82**, 53-95.
- BERNAL, L. P. & ROSHKO, A. 1986 Streamwise Vortex Structure in Plane Mixing Layers. *J. Fluid Mech.* **170**, 499-525.
- BRADSHAW, P. 1966 The Effect of Initial Conditions on the Development of a Free Shear Layer. *J. Fluid Mech.* **26**, 225-236.
- BREIDENTHAL, R. 1981 Structure in Turbulent Mixing Layers and Wakes Using a Chemical Reaction. *J. Fluid Mech.* **109**, 1-24.

- BROWAND, F. G. & LATIGO, B. O. 1979 Growth of the Two-Dimensional Mixing Layer from a Turbulent and a Non-Turbulent Boundary Layer. *The Physics of Fluids*. **22**, no 6, 1011-1019.
- BROWN, G. L. & ROSHKO, A. 1974 On Density Effects and Large Structure in Turbulent Mixing Layers. *J. Fluid Mech.* **64**, 775-816.
- DAHM, W. J. A. 1985 *Experiments on Entrainment, Mixing and Chemical Reactions in Turbulent Jets at Large Schmidt Number*. Ph.D. Thesis, Caltech.
- DIMOTAKIS, P. E., & BROWN, G. L. 1976 The Mixing Layer at High Reynolds Number: Large-Structure Dynamics and Entrainment. *J. Fluid Mech.* **78**, 535-560.
- HUANG, L.-S. & HO C.-M. 1990 Small Scale Transition in a Plane Mixing Layer. *J. Fluid Mech.* **210**, 475-500.
- JIMENEZ, J., COGOLLOS, M. & BERNAL, L. P. 1985 A Perspective View of the Plane Mixing Layer. *J. Fluid Mech.* **152**, 125-143.
- KARASSO, P. S. & MUNGAL, M. G. 1990 An Experimental Study of Curved Mixing Layers: Flow Visualizations Using Volume Rendering. *CTR Annual Research Briefs*, Stanford Univ./NASA-Ames.
- KONRAD, J. H. 1977 *An Experimental Investigation of Mixing in Two-Dimensional Turbulent Shear Flows with Applications to Diffusion-Limited Chemical Reactions*. Ph.D. Thesis, Caltech.
- KOOCHESFAHANI, M. M. & DIMOTAKIS, P. E. 1986 Mixing and Chemical Reactions in a Turbulent Mixing Layer. *J. Fluid Mech.* **179**, 83-112.
- KYCHAKOFF, G., HOWE, R. D. & HANSON, R. K. 1984 Quantitative Flow Visualization Technique for Measurements in Combustion Gases. *Applied Optics*. **23** (5), 704-712.
- LASHERAS, J. C. & CHOI, H. 1988 3-D Instabilities of a Plane Free Shear Layer: An Experimental Study of the Formation and Evolution of Streamwise Vortices. *J. Fluid Mech.* **189**, 53-86.
- MUNGAL, M. G., HERMANSON, J. C. & DIMOTAKIS, P. E. 1985 Reynolds Number Effects on Mixing and Combustion in a Reacting Shear Layer. *AIAA J.* **23** (9), 1418-1423.
- PRINGSHEIM, P. 1949 *Fluorescence and Phosphorescence*. Interscience Publishers, Inc.
- WALKER, D. A. 1987 A Fluorescence Technique for Measurement of Concentration in Liquids. *J. Phys. E.* **20**, 217-224.